RESEARCH ARTICLE | DECEMBER 15 1990

Device modeling of ferroelectric capacitors

S. L. Miller; R. D. Nasby; J. R. Schwank; M. S. Rodgers; P. V. Dressendorfer

J. Appl. Phys. 68, 6463–6471 (1990)
https://doi.org/10.1063/1.346845

Device modeling of ferroelectric capacitors

S. L. Miller, R. D. Nasby, J. R. Schwank, M. S. Rodgers, and P. V. Dressendorfer
Division 2144, Sandia National Laboratories, P. O. Box 5800, Albuquerque, New Mexico 87185

(Received 30 July 1990; accepted for publication 31 August 1990)

A physically based methodology is developed for modeling the behavior of electrical circuits containing nonideal ferroelectric capacitors. The methodology is illustrated by modeling the discrete ferroelectric capacitor as a stacked dielectric structure, with switching ferroelectric and nonswitching dielectric layers. Electrical properties of a modified Sawyer–Tower circuit are predicted by the model. Distortions of hysteresis loops due to resistive losses as a function of input signal frequency are accurately predicted by the model. The effect of signal amplitude variations predicted by the model also agree with experimental data. The model is used as a diagnostic tool to demonstrate that cycling degradation, at least for the sample investigated, cannot be modeled by the formation of nonswitching dielectric layer(s) or the formation of conductive regions near the electrodes, but is consistent with a spatially uniform reduction in the number of switching dipoles.

I. INTRODUCTION

Interest in ferroelectric capacitor structures is increasing due to their recent utilization as the memory element of a new type of integrated circuit nonvolatile memory.[1-3] Electrical properties of ferroelectric capacitor structures are typically determined by making electrical measurements using characterization circuits, such as the Sawyer–Tower test circuit,[4] which contains the capacitor as a circuit element. Unfortunately, the quantitative determination of basic ferroelectric capacitor device properties from typical measurement circuits is very difficult when the capacitor is not "ideal."[5,6] Parasitic effects due to the characterization circuit, as well as resulting from the ferroelectric circuit element itself, can make interpretation of the measurements difficult.

Little has been published regarding quantitative modelling of the electrical behavior of circuits containing thin-film ferroelectric capacitors. Scott *et al.* have investigated the switching kinetics of potassium nitrate and lead zirconate titanate thin films,[7,8] successfully applying the theory of Ishibashi[9] to describe the transient switching currents. Application of the results to model the behavior of circuits containing ferroelectric capacitor elements was apparently not pursued. The authors have recently become aware of a modeling effort by Evans and Bullington,[10] who model hysteresis loops by treating the dipole switching process as resulting from a statistical distribution of switching fields for each dipole. Though this is a useful approach, it does not appear to be amenable to modelling effects resulting from trapped space-charge, nonswitching dielectric layers, or other nonideal physical properties of the ferroelectric.

Motivated by the need to quantitatively characterize nonideal ferroelectric capacitors, as well as the need to accurately predict (not just fit) ferroelectric integrated circuit response, we have developed a technique to model ferroelectric capacitor and circuit properties, including hysteresis effects, which takes into account parasitic properties. The resulting modelling approach provides a means to gain insight into the nature of degradation mechanisms. Fabrication process optimization may also be facilitated, since variations in process parameters and techniques may be correlated with ferroelectric capacitor device properties.

The approach we have taken to model the behavior of ferroelectric capacitors in electrical circuits consists of a procedure with four major steps: (1) define a physical model of the ferroelectric capacitor, including parasitic features, (2) based on the physical model, derive equations relating the charge on the capacitor electrodes to the voltage drop across the capacitor (this results in the definition of a ferroelectric capacitor circuit "element" or "module"), (3) insert the ferroelectric "module" into a circuit of interest, and solve the circuit equations for desired parameters, such as currents and voltages, and finally (4) experimentally verify the solutions, refining the original physical model if necessary. Depending on the accuracy required, the physical model may need to be iterated until the model predictions sufficiently match the experimentally observed results.

The first three steps of the procedure are illustrated in Sec. II. The experimental verification of resulting solutions is then presented in Sec. III. Application of the model as a diagnostic tool is illustrated in Sec. IV, with cycling degradation (fatigue) being the illustration vehicle. A discussion follows in Sec. V in which refinements to the physical model presented are proposed. Applications of the modeling approach are also discussed.

II. THEORY

A. Ferroelectric capacitor module

There are a wide variety of physical features one might wish to include in a model of a ferroelectric capacitor. Our approach is to begin by defining a fairly simple physical model, to develop the mathematical techniques required for implementing the model, and then to refine the physical model as needed to be consistent with experimental results.

The physical model being considered is illustrated in Fig. 1. The capacitor electrodes are separated by a distance of d_f; the area of each electrode is A_f. The electrodes could possibly physically or electrically interact with the ferroelec-

 0021-8979/90/246463-09$03.00

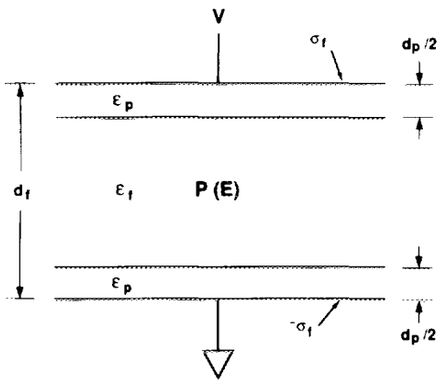

FIG. 1. Physical model of a ferroelectric capacitor circuit element containing a switching ferroelectric layer and nonswitching dielectric layers adjacent to the electrodes.

tric material; hence we include in our physical model two nonswitching dielectric layers, one adjacent to each electrode, and each with a thickness $d_p/2$ and dielectric constant ϵ_p. For an ideal ferroelectric capacitor, d_p is simply zero. The electrical behavior of the capacitor is independent of whether the nonswitching dielectric occurs as a single layer or as multiple layers, provided the total physical thickness is held constant. The remaining dielectric consists of a switching ferroelectric whose dipole polarization is a function of the field and previous history, and whose linear dielectric constant is designated by ϵ_f. A voltage V is applied across the capacitor electrodes. Each electrode has a free surface charge per unit area whose magnitude is σ_f. With these definitions, we proceed to develop the equations which define the relationship between the applied voltage and the charge on the capacitor electrodes.

The electric displacement vector **D** in the ferroelectric layer is perpendicular to the plane of the electrodes, and is defined by

$$D = \epsilon_0 E_f + P_{\text{tot}},$$

where E_f is the electric field in the ferroelectric and P_{tot} is the total ferroelectric polarization. The total polarization can be written as the sum of the linear contribution to the displacement and the contribution due to switching dipoles in the ferroelectric film:

$$D = \epsilon_0 E_f + \epsilon_0 \chi_f E_f + P_d = \epsilon_0 \epsilon_f E_f + P_d, \tag{1}$$

where χ_f is the electric susceptibility of the ferroelectric, $\epsilon_f = 1 + \chi_f$ is the linear dielectric constant of the ferroelectric, ϵ_0 is the permittivity of free space, and P_d is the contribution to the polarization due to switching dipoles only.

Utilizing Maxwell's first equation,

$$\nabla \cdot \mathbf{D} = \rho, \tag{2}$$

it can be shown that the electric field in the ferroelectric and the magnitude of the charge on the capacitor electrodes are given by

$$E_f = \frac{1}{d_f \gamma_1}\left(V - \frac{d_p P_d}{\epsilon_0 \epsilon_p}\right) \tag{3}$$

and

$$\sigma_f = \frac{1}{\gamma_1}\left[\frac{\epsilon_0 \epsilon_f V}{d_f} + P_d\left(1 - \frac{d_p}{d_f}\right)\right], \tag{4}$$

where γ_1 is defined by

$$\gamma_1 = 1 - \frac{d_p}{d_f}\left(1 - \frac{\epsilon_f}{\epsilon_p}\right). \tag{5}$$

The behavior of circuits containing hysteretic ferroelectric elements is dependent on the previous history of the circuit parameters. Thus, the quantities of interest will be parameterized in terms of time. Once the circuit parameters are defined at one point in time, circuit parameters at future times are calculated by integrating from the initial boundary conditions, i.e., by summing the incremental changes in the parameters. To facilitate subsequent computations, Eqs. (3) and (4) must be differentiated with respect to time. But first, we discuss a subtle issue associated with the process of differentiating these equations.

How one evaluates the total differential dP_d/dt depends on the parameters of which P_d is a function, i.e., the physical nature of the polarization. The polarization is a function of the electric field, which itself is a function of time. When an electric field is applied, the polarization does not track the field instantaneously, but lags slightly in time; hence the polarization is also an explicit function of time. Thus the derivative is written as

$$\frac{dP_d(E,t)}{dt} = \frac{\partial P_d(E,t)}{\partial E}\frac{\partial E}{\partial t} + \frac{\partial P_d(E,t)}{\partial t}. \tag{6}$$

For application to the experimental examples considered later, it is assumed the polarization responds to the electric field within a time interval which is very short compared to the time scale over which other relevant parameters change. Specifically, the time constant for dipole switching is assumed to be much shorter than the time required for the applied voltage or internal fields to change appreciably. Thus, the second term on the right-hand side will be omitted in subsequent equations. If this condition is not met, as might be the case for ferroelectric elements in a high-speed integrated circuit, the second term must be included.

Differentiating Eqs. (3) and (4), utilizing Eq. (6), and eliminating the term $\partial E/\partial t$, one obtains

$$\frac{dE_f}{dt} = \frac{dV}{dt}\frac{1}{d_f \gamma_2} \tag{7}$$

and

$$\frac{d\sigma_f}{dt} = \frac{dV}{dt}\frac{\epsilon_0 \epsilon_f}{d_f \gamma_2}\left(1 + \frac{1}{\epsilon_0 \epsilon_f}\frac{\partial P_d(E,t)}{\partial E}\right), \tag{8}$$

where γ_2 is defined by:

$$\gamma_2 = 1 - \frac{d_p}{d_f}\left[1 - \frac{\epsilon_f}{\epsilon_p}\left(1 + \frac{1}{\epsilon_0 \epsilon_f}\frac{\partial P_d(E,t)}{\partial E}\right)\right]. \tag{9}$$

If the dipole polarization is known as a function of the electric field, Eqs. (3) and (4) [or equivalently Eqs. (7) and (8)] unambiguously define the relationship between the voltage applied across the ferroelectric capacitor and the free charge on the capacitor electrodes. The electric-field dependence of the dipole polarization will be discussed later in Sec. II D.

B. Sawyer–Tower circuit

A common characterization circuit utilized to study ferroelectric capacitors is the Sawyer–Tower circuit,[4] or modifications thereof. A slightly modified version of the circuit shall be modeled, as illustrated in Fig. 2. A time-dependent input voltage $V_i(t)$ is applied to the circuit, resulting in an output voltage $V_o(t)$. The resistor $R_f(t)$ simulates the effect of current leakage through a ferroelectric capacitor with finite resistivity. The resistor $R_n(t)$ might represent the input impedence of the instrument utilized to measure the output voltage, or perhaps current leakage through the integrating capacitor. The goal is now to develop the circuit equations which give the output voltage as a function of the input voltage and the parameters associated with the circuit elements.

The charge at node * in Fig. 2 is the sum of the charge on the bottom and top electrodes of the ferroelectric and integrating capacitors, respectively. At any time, this total charge is equal to the charge due to current flowing through the resistors $R_f(t)$ and $R_n(t)$, plus the total charge on the capacitors which existed before any current flow occurred. This condition is defined mathematically by

$$-\sigma_f(t)A_f + \sigma_n(t)A_n = \int_{t_0}^{t} \frac{V_i(t) - V_o(t)}{R_f(t)}\,dt - \int_{t_0}^{t} \frac{V_o(t)}{R_n(t)}\,dt + Q_0. \tag{10}$$

Taking the time derivative of Eq. (10), utilizing Eq. (8), and noting that $\sigma_n(t)A_n = C_n V_o(t)$ (where C_n and A_n are the capacitance and area of the normal capacitor) one arrives at

$$\frac{dV_o(t)}{dt} = \frac{\gamma_3 C_f[dV_i(t)/dt] + [V_i(t)/R_f(t)] + V_o(t)\{[1/R_n(t)] + [1/R_f(t)]\}}{C_n + \gamma_3 C_f}, \tag{11}$$

where

$$\gamma_3 = \frac{1}{\gamma_2}\left(1 + \frac{1}{\epsilon_0 \epsilon_f}\frac{\partial P_d(E,t)}{\partial E}\right) \tag{12}$$

and

$$C_f = (\epsilon_0 \epsilon_f / d_f) A_f. \tag{13}$$

Equation (11) now completes the set of equations required to describe the modified Sawyer–Tower circuit in Fig. 2 containing the ferroelectric capacitor illustrated in Fig. 1. A technique to solve the equations is described in the following section.

C. Numerical integration algorithm

For specified initial conditions, the output voltage as a function of time can be determined by solving the coupled set of algebraic and differential equations (3) and (11). It is assumed the function $\partial P_d/\partial E$ is known as a function of the field E (this function will be discussed in the next section), and the input voltage $V_i(t)$ is known as a function of time. After each increment in time, the following quantities are calculated: P_d, $\partial P_d/\partial E$, E_f, $V_o(t)$, and $dV_o(t)/dt$. A numerical integration algorithm for this calculation is now discussed. Although alternative computational procedures exist, the algorithm outlined below has been found to be easily implemented and to work over a wide range of parameters.

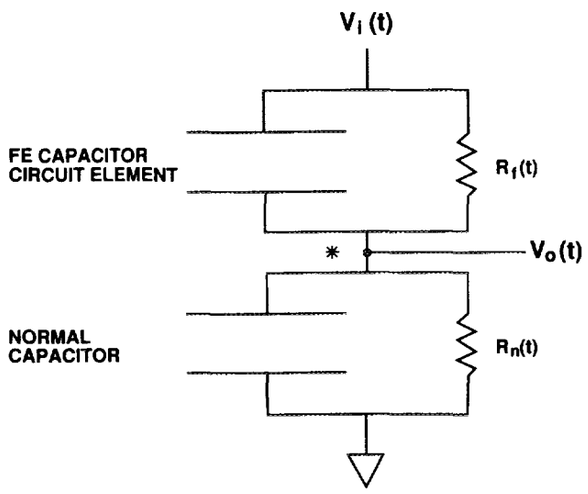

FIG. 2. Modified Sawyer–Tower circuit with parasitic resistances.

The initial conditions consist of the specification, at some initial value of time, of the dipole polarization P_d, the output voltage V_o, the input voltage V_i, and the derivative dV_i/dt. The field at that time is then calculated using

$$E_f = \frac{1}{d_f \gamma_1}\left(V_i - V_o - \frac{d_p P_d}{\epsilon_0 \epsilon_p}\right). \tag{14}$$

Knowing the field, dP_d/dE can be computed. Finally, dV_o/dt is calculated from Eq. (11). Once the initial values of these necessary functions are determined, the time is then incremented. The procedure to compute the above quantities for the lth increment in time is now discussed.

The input voltage V_i and dV_i/dt are known by definition. The output voltage at the lth increment in time is given by

$$V_{o_l} = V_{o_{l-1}} + \frac{dV_o}{dt_{l-1}}(t_l - t_{l-1}). \tag{15}$$

The field is calculated by observing that Eq. (14) can be written as

$$E_{f_l} = \frac{1}{d_f \gamma_1}\left[V_{i_l} - V_{o_l} - \frac{d_p}{\epsilon_0 \epsilon_p}\left(P_{d_{l-1}} + \frac{dP_d}{dE_{l-1}} \times (E_{f_l} - E_{f_{l-1}})\right)\right]. \tag{16}$$

Solving Eq. (16) for the value of the field at the lth increment, we obtain

$$E_{f_l} = \frac{V_{i_l} - V_{o_l} - (d_p/\epsilon_0\epsilon_p)\left[P_{d_{l-1}} - (dP_d/dE_{l-1})E_{f_{l-1}}\right]}{d_f\gamma_1 + (d_p/\epsilon_0\epsilon_p)(dP_d/dE_{l-1})} \tag{17}$$

The dipole polarization is calculated using

$$P_{d_l} = P_{d_{l-1}} + \frac{dP_d}{dE_{l-1}}(E_{f_l} - E_{f_{l-1}}). \tag{18}$$

The lth value of dP_d/dE is then calculated utilizing the appropriate algorithm (to be discussed below). Finally, the lth value of dV_o/dt is calculated from Eq. (11).

After the initial values of the functions are determined, the procedure defined in the above paragraph is applied repeatedly to determine the behavior of the circuit as a function of time.

D. Determination of dP_d/dE

The equations developed above can be solved only if the derivative of the dipole polarization with respect to the electric field is known. Before writing an explicit expression for this quantity, we first state some basic physical properties of the dipole polarization, as well as some definitions. As the field is ramped between large absolute values opposite in sign, the switching dipole polarization P_d must approach the asymptotic values of $\pm P_s$, where P_s is the spontaneous polarization. P_s is the polarization which results when all the dipoles are fully aligned. The resulting field-dependent polarization is referred to as the saturated polarization loop (saturated in the sense that the field is ramped between values sufficiently large that essentially all the dipoles switch in both directions). This behavior is illustrated in Fig. 3. The saturated polarization has zero magnitude at a value of the electric field called the coercive field, E_c. At zero field, the value of the saturated polarization is P_r, the remanent polarization. We make the physical assumption that the two branches of the saturated switching dipole polarization curve are symmetric. This assumption is expressed by

$$P_d(E) = -P_d^-(-E), \tag{19}$$

where the plus (+) sign indicates the branch of the polarization for the positive-going field ramp and the minus (−) sign indicates the branch for the negative-going field ramp.

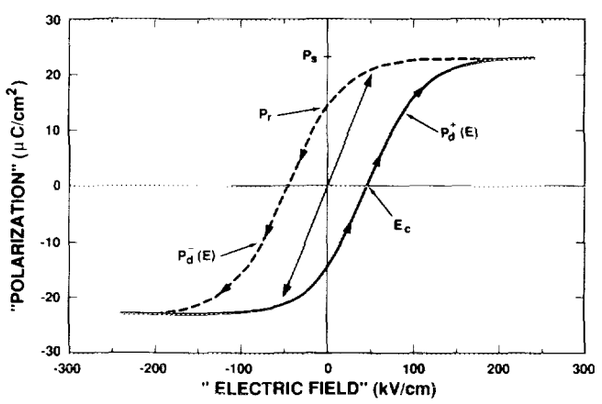

FIG. 3. Model for switched dipole polarization, computed from Eqs. (19) and (20). The polarization saturates at $\pm P_s$.

In the absence of a fundamental physical theory which predicts dipole switching properties as a function of applied field, the saturated polarization $P_d^+(E)$ is defined utilizing a convenient mathematical function whose behavior satisfies the physical requirements. A number of candidate functions exist, among them being the error function (an integral of a Gaussian distribution),[11] the Langevin function encountered in magnetism,[12] and the hyperbolic tangent function.[13] The hyperbolic tangent function is chosen due to its convenient mathematical properties. As will be shown later, this choice of function is consistent with experimental data. (It is emphasized that the equations developed up to this point are independent of the specific choice of the function to describe the field dependent saturated dipole polarization.) Specifically, the saturated polarization loop is defined by

$$P_d^+(E) = P_s \tanh[(E - E_c)/2\delta], \tag{20}$$

where

$$\delta = E_c\left[\log\left(\frac{1 + P_r/P_s}{1 - P_r/P_s}\right)\right]^{-1}, \tag{21}$$

and P_r, P_s, and E_c are taken as positive quantities. The constant δ is defined such that $P_d^+(0) = -P_r$. The negative branch of the saturated switching dipole polarization is given by Eq. (19). Differentiating Eq. (20), one obtains

$$\frac{dP_d^+(E)}{dE} = P_s\left[2\delta\cosh^2\left(\frac{E - E_c}{2\delta}\right)\right]^{-1} \tag{22}$$

and

$$\left.\frac{dP_d^-(E)}{dE}\right|_E = \left.\frac{dP_d^+(E)}{dE}\right|_E. \tag{23}$$

The derivative of the switching dipole polarization with respect to the ferroelectric electric field is given, for the case where the polarization is saturated, by Eqs. (22) and (23). What happens if the applied signal does not drive the polarization into saturation? Existing data indicate that the derivative of the polarization with respect to the field, evaluated at a constant field, is independent of the amplitude of the applied signal, at least to first order. Hence, the assumption is now made that the derivatives defined in Eqs. (22) and (23) are independent of the amplitude of the oscillating electric field. Figure 4 illustrates a family of polarization curves generated by Eqs. (22) and (23) for several different electric-field amplitudes. Note that the slope at a given field is the same for each curve.

III. RESULTS

A. Experimental procedures

To examine the validity of the modelling approach discussed thus far, the circuit illustrated in Fig. 2 was assembled. A ferroelectric capacitor fabricated with the sol-gel process, of area 10 000 μm^2 and thickness 400 nm, was utilized. The normal "integrating" capacitor had a capacitance of 10 nF. A high-speed digitizer was utilized to measure the input and output voltages $V_i(t)$ and $V_o(t)$; the input impedence was 1 MΩ $= R_n(t)$. The input signal was a symmetric

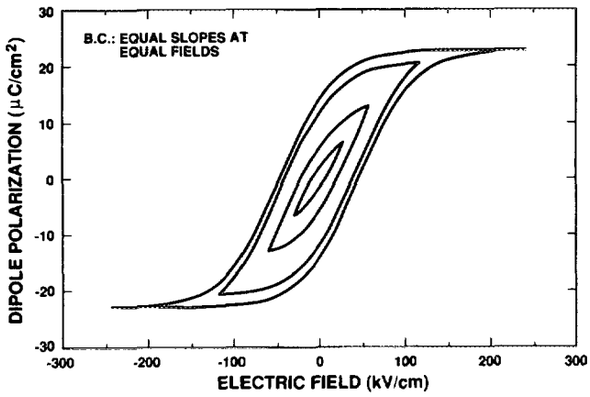

FIG. 4. Family of unsaturated switched dipole polarization hysteresis loops, computed from Eqs. (22) and (23). The slope of a given branch at a given value of electric field is independent of the amplitude of the symmetric periodic field.

sine wave with adjustable frequency and amplitude. A given set of data was obtained by first applying 500 cycles to the circuit, then digitizing the input and output voltages for the 501st cycle.

Though the resulting data may be graphically represented by plotting the voltages as a function of time, we choose to plot the output voltage as a function of the input voltage. Specifically, we plot on the x axis the quantity

$$X(t) = V_i(t)/d_f \tag{24}$$

and on the y axis the quantity

$$Y(t) = V_o(t)C_n/A_f. \tag{25}$$

The resulting curve is a hysteresis loop; it is a structure which is associated with the entire circuit, rather than simply being associated with the ferroelectric capacitor. The function $X(t)$ is an approximation to the ferroelectric electric field. The function $Y(t)$ is an approximation to the total ferroelectric polarization (linear plus switching contribution). The quantities defined in Eqs. (24) and (25) are what are commonly plotted when characterizing the hysteresis of a ferroelectric capacitor. These approximate expressions for the field and polarization become accurate only in the limit where the capacitance of the normal capacitor is large compared to that of the ferroelectric, when the current flowing through the resistors is small compared to the capacitor displacement currents, and if the capacitance of nonswitching layers is very large compared to that of the ferroelectric dielectric layer. Thus, the axes for hysteresis plots will be labeled "Electric Field" and "Polarization," the quotes indicating that the values plotted do not necessarily correspond to the true ferroelectric field and the true polarization. The parameters utilized in the following experiments span a sufficiently wide range that Eqs. (24) and (25) are not always valid approximations to the actual ferroelectric field and polarization.

B. Determination of model parameters

The next step in verifying the validity of the circuit equations for the circuit in Fig. 2 is to determine the parameters P_r, P_s, E_c, and ϵ_f for the ferroelectric capacitor. A hysteresis loop was obtained utilizing a sine wave input with a 10-V amplitude (20 V peak to peak), driving the capacitor into saturation. A frequency of 100 kHz was utilized to minimize effects due to resistive losses. Values of $P_r = 14\ \mu\text{C/cm}^2$, $P_s = 23\ \mu\text{C/cm}^2$, $E_c = 45$ kV/cm, and $\epsilon_f = 600$ were determined by fitting the model prediction to the hysteresis loop. (This value of ϵ_f results in a computed value of 132 pF for the linear capacitance of the ferroelectric capacitor.) These parameters, along with a value of $d_p = 0$ and $R_f(t) \to \infty$, were utilized as inputs to the model, and the solid curve in Fig. 5 was generated using the computational algorithm discussed in Sec. II. The dots are the experimental data.

The good agreement between the model results and the experimental data indicates that the physical description of the ferroelectric capacitor is reasonable, the computational algorithm works properly, and the physical parameters are correctly chosen. Next, the values of the circuit parameters are varied to see whether or not the resulting circuit behavior is accurately predicted. No further adjustments to the ferroelectric parameters are made; the only changes to the model input parameters will be known parameters associated with the input signal and circuit elements.

C. Effects of digitizer impedance

The finite digitizer impedance can significantly impact the resulting hysteresis loop when the signal frequency is sufficiently low. Distortion occurs when the charge flowing through the digitizer per input signal cycle is not negligible compared to the charge on the integrating capacitor. A hysteresis loop obtained at a frequency of 100 Hz is shown in Fig. 6. Very good agreement is observed between the predicted hysteresis loop and the experimental data. The only model parameter which was changed from the set which generated the curve in Fig. 5 was the frequency.

A series of hysteresis loops was then obtained at different frequencies. A plot of the apparent "remanent polarization," i.e., the total "polarization" at zero field, as a function of signal frequency is shown in Fig. 7. Again, very good

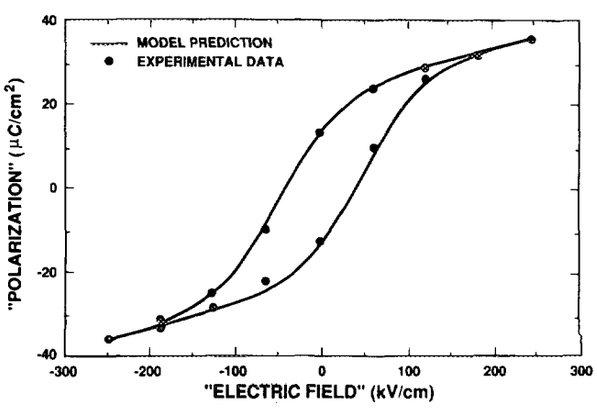

FIG. 5. Hysteresis loops with model parameters extracted from experimental data. Resulting model calculations closely match the data.

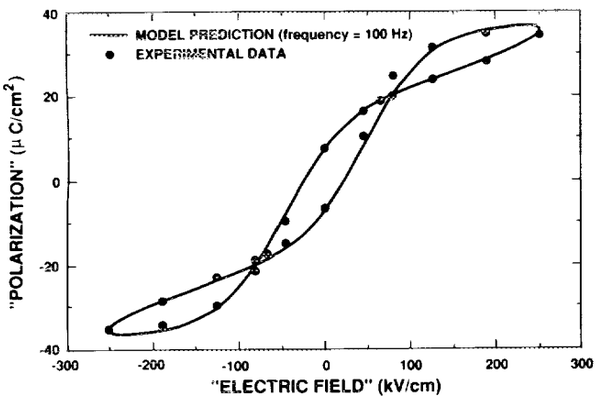

FIG. 6. Characteristic hysteresis loop resulting from resistive leakage through $R_{\prime\prime}$. The model (with no adjustable fitting parameters) accurately predicts the experimental data.

agreement between the model prediction and the experimental data is observed. The apparent reduction in the remanent polarization is an artifact of the choice of circuit parameters; full switching of the ferroelectric still occurs. The true ferroelectric remanent polarization P_r is a property of the ferroelectric capacitor itself, and not a property of the characterization circuit. The distortion at low frequencies resulting from the finite impedence of the digitizer can also arise if the normal capacitor has a finite resistive component to its impedence.

D. Effects of ferroelectric resistive leakage

The hysteresis loop can experience another type of frequency dependent distortion if the resistivity of the ferroelectric capacitor is not infinite. Since we could not physically change the resistivity of the ferroelectric capacitor under study, we simulated the existence of a finite resistivity by the addition of a resistor in parallel with the ferroelectric capacitor. Its value was 1.1 MΩ = $R_f(t)$, equivalent to a value of 3×10^6 Ω cm for the resistivity of the ferroelectric capacitor dielectric. Figure 8 shows resulting hysteresis loops obtained at frequencies of 100 and 1 kHz. The only model parameters which were changed to generate the solid theoretical curves were the known values of the resistance $R_f(t)$ and the frequency. As before, the experimental data are accurately predicted.

A series of hysteresis loops was obtained at additional frequencies. In Fig. 9, a plot of the apparent "remanent polarization" as a function of signal frequency indicates good agreement between the model prediction and the experimental data. This time, the apparent "remanent polarization" increases at lower frequencies, rather than decreases. As before, this behavior is an artifact of the nature of the characterization circuit. Full switching of the ferroelectric still occurs.

E. Effects of signal amplitude

In addition to frequency, the amplitude of the input signal affects the observed circuit hysteresis loops. Hysteresis loops were obtained for a range of amplitudes; the resulting "coercive field" (value of the field at zero polarization) is plotted in Fig. 10 as a function of amplitude. The resistor $R_f(t)$ was removed from the circuit for this series of experiments. The experimentally observed rapid increase and subsequent saturation of the "coercive field" is predicted by the model. As before, no adjustable parameters were utilized to obtain the good fit; the solid curve was generated by the model by changing only the value of the signal amplitude.

IV. USE OF MODEL AS A PHYSICAL DIAGNOSTIC TOOL

Up to this point, we have verified that the model accurately predicts the effects resulting from known changes in the values of the circuit elements and input signal parameters. The good agreement between model predictions and experimentally observed results supports the modelling approach as being correct. Now we are in a position to utilize the model as a diagnostic tool, i.e., to infer information re-

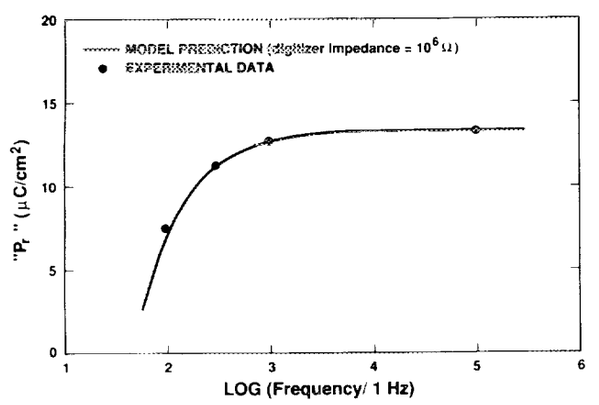

FIG. 7. The apparent "remanent polarization", as defined by Eq. (25) at zero field, decreases with decreasing frequency for finite resistance $R_{\prime\prime}$. The true remanent polarization differs from that plotted. The experimental results are accurately predicted by the model.

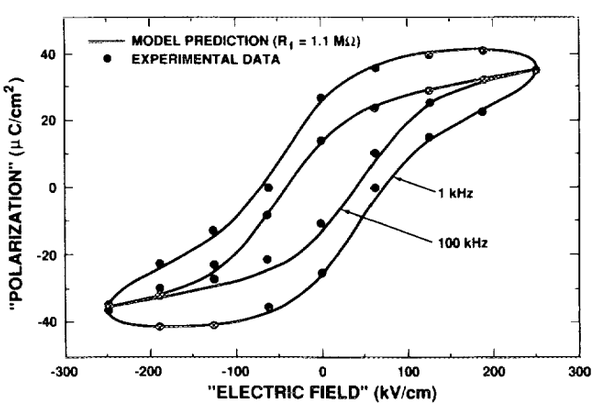

FIG. 8. Characteristic hysteresis loops resulting from resistive leakage through R_f. The model (with no adjustable fitting parameters) accurately predicts the experimental data.

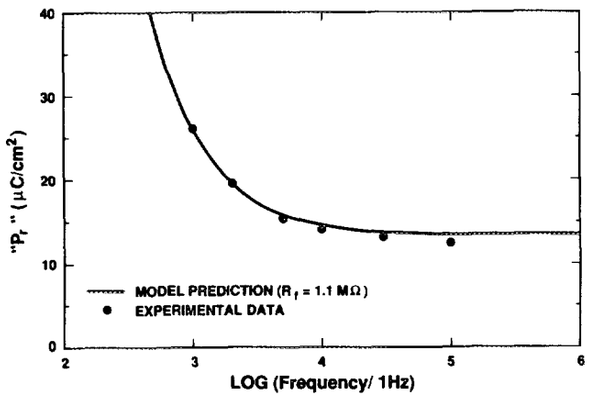

FIG. 9. Apparent "remanent polarization," as defined by Eq. (25) at zero field, increases with decreasing frequency for finite R_f. The true remanent polarization differs from that plotted. The experimental results are accurately predicted by the model.

garding the physical properties of the ferroelectric capacitor from measurements obtained from the test circuit.

As an example of utilizing the model as a diagnostic tool, we consider changes in the electrical response of the ferroelectric capacitor resulting from repeated polarization reversal cycling, often referred to as fatigue. The focus of the following discussion is to illustrate the use of the model as a physical diagnostic tool, and not to develop or establish a comprehensive microscopic theory of cycling degradation.

Hysteresis loops before cycling degradation had occurred, and after 4×10^9 cycles, are shown in Fig. 11(a). Model parameters were obtained from the predegradation data, and were utilized to theoretically generate the solid curve. After cycling, the apparent switched charge in the ferroelectric capacitor is significantly reduced. The basic question is: what physically has changed in the capacitor to result in the different hysteresis loop? The approach to answer this question is to make an assumption, and then see whether or not the model prediction is consistent with the

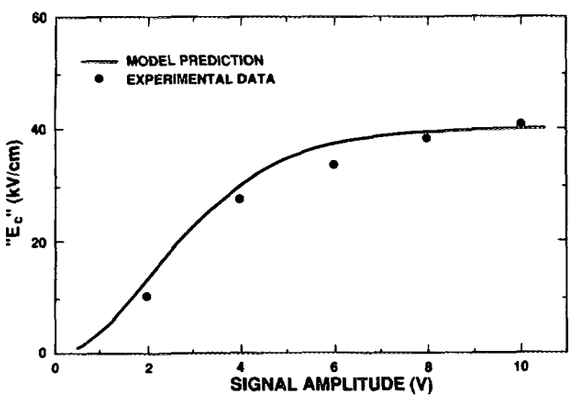

FIG. 10. Observed coercive field, defined utilizing Eq. (24) at zero polarization, decreases with decreasing signal amplitude. The model prediction agrees with the experimental data.

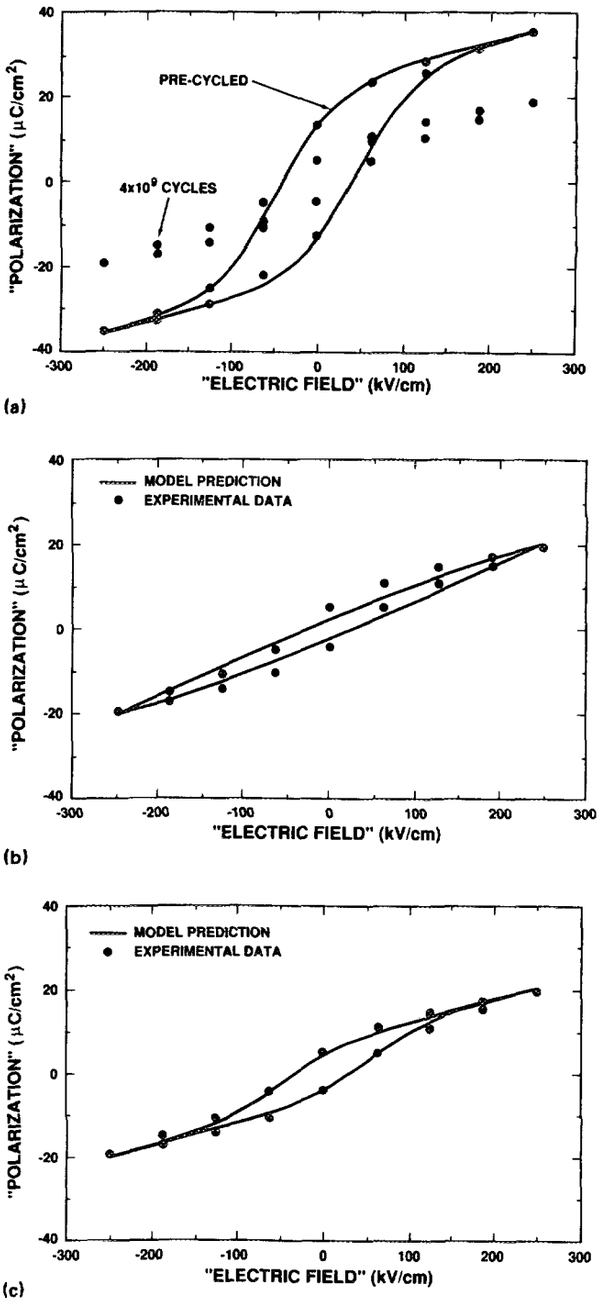

FIG. 11. Physical effect of cycling degradation is examined utilizing the model. (a) Pre- and post-cycling degradation hysteresis data. Physical parameters are determined from the predata. (b) Post-cycled data is not accurately predicted by assuming the presence of a nonswitching dielectric layer. (c) Post-cycled data is accurately predicted by assuming a spatially uniform reduction in the number of switching dipoles.

observed results. If the prediction is inconsistent, the assumption is wrong. If the prediction is consistent, the assumption may be correct.

We begin by assuming that the cycling resulted in some interaction between the electrodes and the ferroelectric material which caused the formation of a nonswitching region of the ferroelectric near the electrodes. Several mechanisms

have been proposed by which a nonswitching layer could occur. It has been proposed that cycling results in an increase in the space-charge region near the electrodes, causing a reduction in the switching of the dipoles in the affected regions.[14] Another proposed effect of cycling is the formation of conductive dendrites growing from the electrodes into the ferroelectric.[15,16] A possible effect of dendritic structures is to shield the domains under the dendritic branches from the applied field, causing them not to switch. Independent of a specific proposed mechanism which might result in a nonswitching dielectric layer, the solid curve in Fig. 11(b) was generated by adjusting the nonswitching dielectric thickness d_p to a value which gave the optimum fit to the data. Rather than preserving the characteristic "S" shape of the hysteresis loop, the existence of a nonswitching dielectric layer collapses the hysteresis loop into a rather structureless oval. (This behavior was also experimentally observed when a normal capacitor was inserted in series with a nondegraded ferroelectric capacitor, and was accurately predicted by the model.) The lack of even qualitative agreement with the experimental post-cycling data indicates that the primary effect of cycling was not to produce a nonswitching dielectric layer(s), either at the electrodes, or elsewhere in the structure.

The existence of conductive dendritic structures eminating from the electrodes could result in an additional type of effect. If the lateral spacing of the dendrite tips is less than the length of the dendrites, as is shown in Ref. 16, the result would be a reduction in the effective thickness of the ferroelectric capacitor. If the effective thickness varied laterally, the resulting switching behavior could be modeled simply by the parallel connection of a large number of small-area capacitors with different thicknesses. The expected first-order consequence would be a scaling of the electric-field axis of the resulting hysteresis loop. The detailed form of the scaling function would depend on the distribution of thicknesses. The post-cycling data in Fig. 11(a) cannot be obtained from the precycling data simply by scaling the field axis, even in a nonlinear way.

Next, we assume that the number of switching dipoles is uniformly reduced throughout the volume of the ferroelectric material as a result of repeated polarization reversals. This could occur as a result of pinning of domain walls.[17] This effect would be simulated by scaling both P_r and P_s to be smaller than their original values by the same scaling factor. The solid curve in Fig. 11(c) was obtained using the precycled parameters (including E_c) with the exception that both P_r and P_s were scaled to values 30% the magnitude of their original values. Observe that the resulting model prediction matches the experimental data quite well over the entire hysteresis loop. The slight discrepancy at large values of the field may be due to losses resistive in nature. One concludes that a uniform reduction in the number of switching dipoles is a plausible and consistent explanation for the observed change in electrical behavior due to cycling degradation for the sample investigated.

We have not yet verified whether or not these specific results are also obtained with samples processed with different compositions or electrode interfaces. Thus, one must be cautious in making generic conclusions from this very limited data set regarding the physical effects resulting from cycling, and how those physical effects might impact the electrical properties. We have demonstrated the modeling *approach* developed in this paper will certainly be of use in addressing these issues.

V. DISCUSSION

A conceptual and mathematical methodology for modelling the behavior of circuits containing at least one ferroelectric capacitor has been developed. This methodology has been illustrated with a very simplified physical model of the ferroelectric capacitor, which appears to work quite well in predicting experimental results, at least to first order. However, there are a number of refinements one might wish to make to the physical model. For example, one might wish to make the dielectric constants frequency dependent, especially for high-frequency applications. For these applications, one may also need to include the explicit dependence of the dipole polarization on time, as was discussed in Sec. II A. The inclusion of space charge in the ferroelectric layer might provide insight into the response of ferroelectric capacitors to ionizing radiation. Such modifications simply change the relationship between the charge on the ferroelectric capacitor electrodes and the voltage drop across the capacitor. Equations (3) and (4) are replaced by the appropriate expressions; the procedure required to set up and solve the circuit equations is then the same as that developed in the rest of Sec. II.

Another area which might require refinement is the definition of the derivative of the field dependent dipole polarization $dP_d(E)/dE$. Practical integrated circuit applications require the ability to model ferroelectric response to asymmetric and nonperiodic input signals. If the applied voltage does not result in a ferroelectric electric field which ranges between values equal in magnitude, Eqs. (22) and (23) are not adequate. They can result in dipole polarizations which exceed P_s in magnitude, a nonphysical result. A possible approach is to treat the polarization in a manner analogous to the magnetization hysteresis of ferromagnetic materials.[18]

Independent of the specific physical model one utilizes, it is clear from the above examples that the nature of the characterization circuit and signal parameters can significantly impact the inferred results from simple electrical measurements such as hysteresis loops. The actual switched charge and coercive field may be very different from the values obtained by utilizing such simplified Eqs. (24) and (25) to calculate the ferroelectric electric field and switched charge. Thus, values of P_r, P_s, and E_c reported in the literature may be ambiguous unless the parameters associated with the test circuit elements, as well as the nature of the input signal, are specified.

It is possible to perform characterization measurements which are inherently immune to certain types of parasitic effects. For example, regarding errors due to resistive parasitic effects, if the hysteresis loop does not change as a function of frequency over a range of at least one order of magni-

tude, then the frequency is sufficiently high that parasitic resistive effects are negligible. In the other extreme, if the period of the applied signal is not large compared to the actual switching time of the dipoles, the resulting signal will be convoluted with the effects of the finite switching time. In this regime, the second term in Eq. (6) must be included in the mathematical analysis. Procedures to empirically determine whether or not other particular parasitic effects exist can be developed by utilizing the model. To do this, one sequentially varies given input parameters of the model and computes the effect on the electrical circuit parameter of interest.

The ability to easily model ferroelectric circuits allows one the flexibility to design circuits which might be more sensitive or immune to certain effects, or be more appropriate for a given measurement equipment set or application. For example, the conventional Sawyer–Tower characterization circuit typically consists of an integrating capacitor whose capacitance is large compared to that of the ferroelectric capacitor. The equations developed in Sec. II can be used to model a Sawyer–Tower circuit where the capacitance of the integrating capacitor is not large compared to that of the ferroelectric capacitor. If one prefers to characterize a ferroelectric capacitor by numerically integrating the switched current passing through a resistor rather than using an integrating capacitor, one simply lets $C_n \rightarrow 0$ in the above equations; the current is given by $I(t) = V_o(t)/R_n(t)$. Various modifications to the standard Sawyer–Tower test circuit, such as compensated and virtual ground circuits,[6] can also be modeled with the approach described here. A ferroelectric circuit modeling capability is essential in order to accurately model the structures required in an integrated circuit memory cell or sensing circuit.

Additional applications of this modeling approach include understanding the effects of degradation phenomena. Experimentally observed results can be quantitatively related to basic physical properties of the ferroelectric capacitor system. This was illustrated by the above analysis of cycling induced degradation. One could gain further insight into the nature of cycling degradation by plotting the polarization scaling factor as a function of the number of cycles. Utilizing the model to extract such quantities as the remanent polarization or coercive field, one may be able to understand other effects, such as the impact of the cycling amplitude or the consequences of the thermal environment. This modeling approach may also be implemented to optimize certain ferroelectric circuit fabrication procedures; electrical properties are directly related to physical properties which can then be related to fabrication procedures.

VI. SUMMARY

A physically based practical approach has been presented which can be utilized to model the behavior of electrical circuits containing ferroelectric capacitors. The modeling approach may be easily adapted to incorporate essentially any physical model of a ferroelectric capacitor element. The model has been demonstrated for a Sawyer–Tower circuit, accurately predicting the experimentally observed distortions to hysteresis loops resulting from changes in circuit element parameters and input signal frequency and amplitude. The standard approximations used for measurements of the ferroelectric electric field and switched charge, listed in Eqs. (24) and (24), are often invalid. This can result in misleading conclusions regarding the inferred properties of a ferroelectric capacitor characterized with a given test circuit.

The model can be used to provide further insight into the physical mechanisms of ferroelectric operation and degradation. The utility of the model as a physical characterization tool was illustrated by examining the nature of cycling degradation. For the sample considered here, the observed cycling degradation was inconsistent with the development of nonswitching dielectric layers or an effective thinning of the capacitor; it was consistent with a uniform reduction in the number of switching dipoles.

Proper use of this modeling approach can facilitate accurate characterization of ferroelectric elements, and efficient optimization of design integration of ferroelectric devices into semiconductor integrated circuits.

ACKNOWLEDGMENTS

The authors are grateful to G. Goddard and K. Gutierrez for their technical assistance, and to N. Godshall and A. Campbell for critically reviewing the manuscript.

[1] J. F. Scott and C. A. Araujo, Science **246**, 1400 (1989); J. F. Scott and C. A. Araujo, in *Molecular Electronics*, edited by M. Borisson (World Scientific, Singapore, 1986), pp. 206–214.
[2] J. T. Evans and R. Womack, IEEE J. Solid State Circuits **23**, 1171 (1988).
[3] D. Bondurant, in The First Symposium on Integrated Ferroelectrics, University of Colorado, Colorado Springs, 1989, pp. 212–215 (unpublished).
[4] C. B. Sawyer and C. H. Tower, Phys. Rev. **35**, 269 (1930).
[5] M. E. Lines and A. M. Glass, *Principles and Applications of Ferroelectrics and Related Materials* (Oxford University Press, Oxford, 1977), p. 104.
[6] J. T. Evans, M. D. Ivey and J. A. Bullington, in The First Symposium on Integrated Ferroelectrics, University of Colorado, Colorado Springs, 1989, pp. 217–221 (unpublished).
[7] J. F. Scott, L. Kammerdiner, M. Parris, S. Traynor, V. Ottenbacher, A. Shawabkeh, and W. F. Oliver, J. Appl. Phys. **64**, 787 (1988).
[8] J. F. Scott, C. A. Araujo, H. B. Meadows, L. D. McMillan, and A. Shawabkeh, J. Appl. Phys. **66**, 1444 (1989).
[9] Y. Ishibashi, Jpn. J. Appl. Phys. **24**, 126 (1986).
[10] J. A. Bullington and J. T. Evans (private communication).
[11] G. Arfken, *Mathematical Methods for Physicists* (Academic, New York, 1970), p. 474.
[12] J. R. Reitz and F. J. Milford, *Foundations of Electromagnetic Theory* (Addison-Wesley, Reading, MA, 1967), p. 225; D. J. Craik, *Structure and Properties of Magnetic Materials* (Pion, London, 1971), p. 31.
[13] W. H. Beyer, Ed., *CRC Standard Mathematical Tables*, 25th ed. (CRC, Boca Raton, FL, 1979), p. 252.
[14] J. A. Bullington, M. D. Ivey, and J. T. Evans, in The First Symposium on Integrated Ferroelectrics, University of Colorado, Colorado Springs, 1989, pp. 201–211 (unpublished).
[15] R. H. Plumlee, Sandia Laboratories Report No. SC-RR-67-730 (1967).
[16] C. A. Araujo, L. D. McMillan, B. M. Melnick, J. D. Cuchiaro, and J. F. Scott, Ferroelectrics **104**, 241 (1990).
[17] J. F. Scott and B. Pouligny, J. Appl. Phys. **64**, 1547 (1988).
[18] D. C. Jiles, J. Magn. Magn. Mater. **61**, 48 (1986).